Interstellar Organics

About 800,000 years ago a meteor struck near Mount Darwin in Western Tasmania, vapourising large quantities of rock together with the rainforest growing on it. The vapourised rock condensed, falling like rain over an area of about 400 km^2. The condensation rate was very rapid so that the rock had no time to crystallise: it can still be picked up at the site in large volumes as a *glass* with a characteristic morphology, and it is therefore called "***Darwin glass***". As an amorphous (non-crystalline) material, a piece of Darwin glass was used as a standard to set up X-ray diffraction (XRD) equipment in London at the Natural History Museum (NHM): it was therefore very surprising to see from it XRD signals for quartz and rutile (crystalline forms of silica and titania). These were subsequently found to be from inclusions in the glasses (see ***Figures 2 & 3*** for images of the crater, a collection of glasses and a typical inclusion).

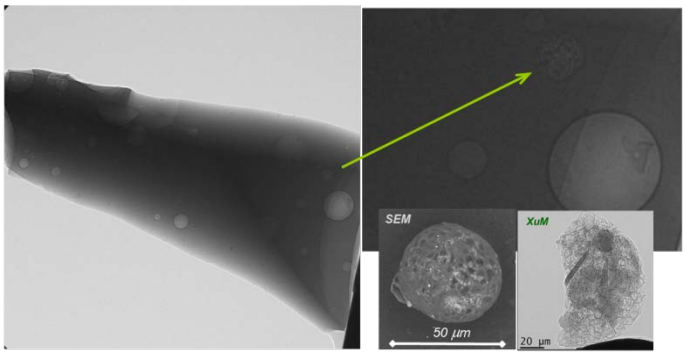

Figure 3: *Morphology of Darwin glass inclusions*
Left: XUM image of a Darwin glass, with voids and inclusions; ***Right:*** arrow indicates (magnified) inclusion; ***Inset:*** SEM and XUM images of extracted inclusions.
SEM: scanning electron microscope. ***XUM:*** X-ray ultramicroscope, an SEM attachment that essentially permits X-ray tomography.
From Figures 1, S5, and movie of Howard et al, *Nature Geoscience* 2013.

The NHM geologist was baffled by the extracted inclusions, being unable to identify them. But ion beam analysis (IBA) using a proton beam of about 2 MeV, immediately identified them as having a carbon matrix from the characteristic $^{12}C(p,p)^{12}C$ elastic resonance at 1734 keV. This was an apparently incredible result, since the impact process involves extremely high temperature temperatures in excess of 1700°C.

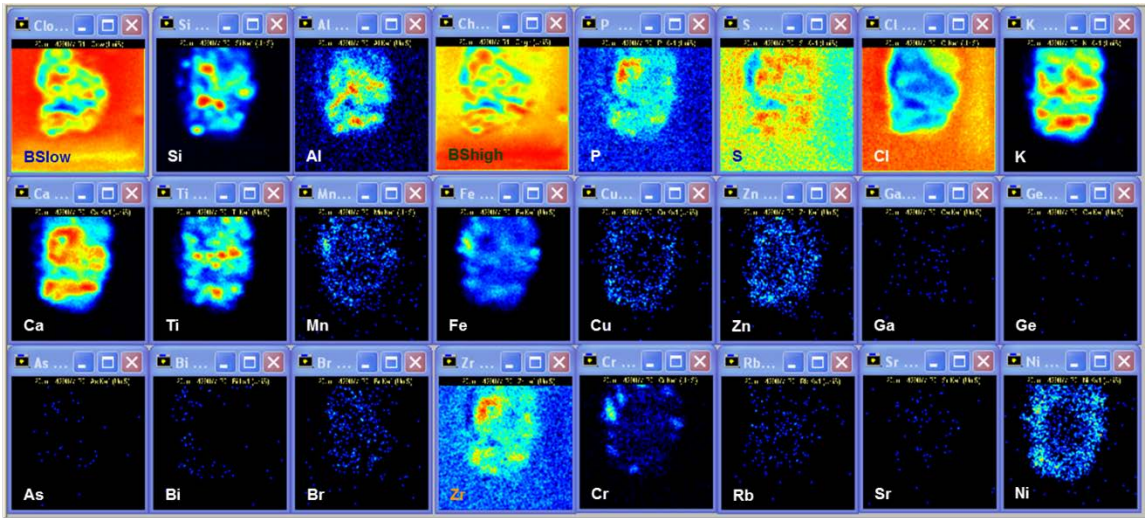

Figure 4: ***IBA maps from a 50 μm inclusion from a Darwin impact glass, set in resin and polished.***
1.9 MeV proton-induced X-ray emission (PIXE) maps for 22 elements, with maps of the low- and high-energy parts of the proton backscattering spectra.

Figure 4 shows highly heterogeneous maps extracted from a large dataset collected while scanning the focussed proton beam over the inclusion imaged in Figure 3. Note that the inclusion is set in resin, which is Cl-rich (penultimate map in top row). Similar datasets were obtained for 1.76 MeV and 2.4 MeV proton beams.

The PIXE and EBS spectra in ***Figure 5*** (Bailey et al, *Nucl. Instruments & Methods B*, 2009 [2]) were extracted from silicon-rich regions of the dataset (see the 2nd map in the top row of Figure 4). EBS spectra for all three beam energies are shown: recall that the carbon resonance occurs at 1.734 MeV so that the resonance is excited near the surface for 1.76 MeV, but progressively deeper in the sample for 1.9 and 2.4 MeV: it is the lowest energy (1.76 MeV) that shows the resonance shape. From this spectrum there is no doubt that carbon is present, in large quantities.

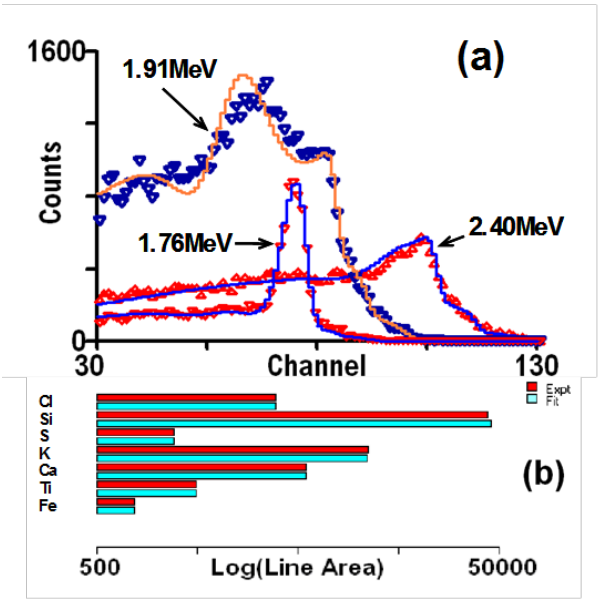

Figure 5: ***Unambiguous identification of inhomogeneous silica in a carbonaceous matrix by IBA.***
(a) Sequential EBS spectra with different beam energies;
(b) Line areas from PIXE spectrum
(c) Derived depth profile (see text)

From Figure 5 in Bailey et al, *NIMB* 2009

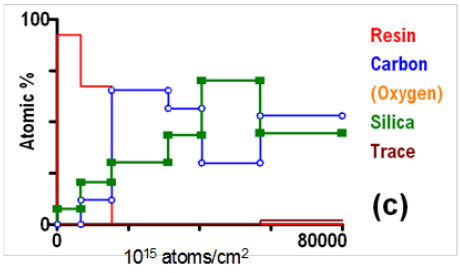

The heterogeneity clear from Figure 4 is central in the interpretation of Figure 5. It is the 1.9 MeV spectrum that is critical here. The carbon content is high, but the resonance shape is strongly attenuated! Assuming a uniform matrix the spectrum cannot be fitted, but it becomes interpretable when a ***non-uniform*** distribution of elements is assumed. It is fitted assuming the Si is all present as an oxide, and that the silica has condensed into precipitates of a certain size. In such a case much larger energy straggling [3] can be calculated, fitting the data fairly well.

The elastic backscattering (EBS) particle spectra are entirely unequivocal when taken together with particle-induced X-ray emission (PIXE), and when the straggling induced by the heterogeneity is included. Figure 5 shows the elemental depth profile obtained when all the spectra (EBS and PIXE) are fitted simultaneously.

The inclusion was set in resin and polished in the way usual for geological samples, and the IBA fitting was in terms of the resin molecule, SiO_2, C and a residue "molecule" to account for the trace elements detected by PIXE. The major elements in this sample are C, O, and Si, all of which are strongly non-Rutherford at these energies.

Note also that XUM tomography was also subsequently used to highlight the pronounced density inhomogeneity of this material: see the inset to Figure 3 which is a still from a movie of the tomograph.

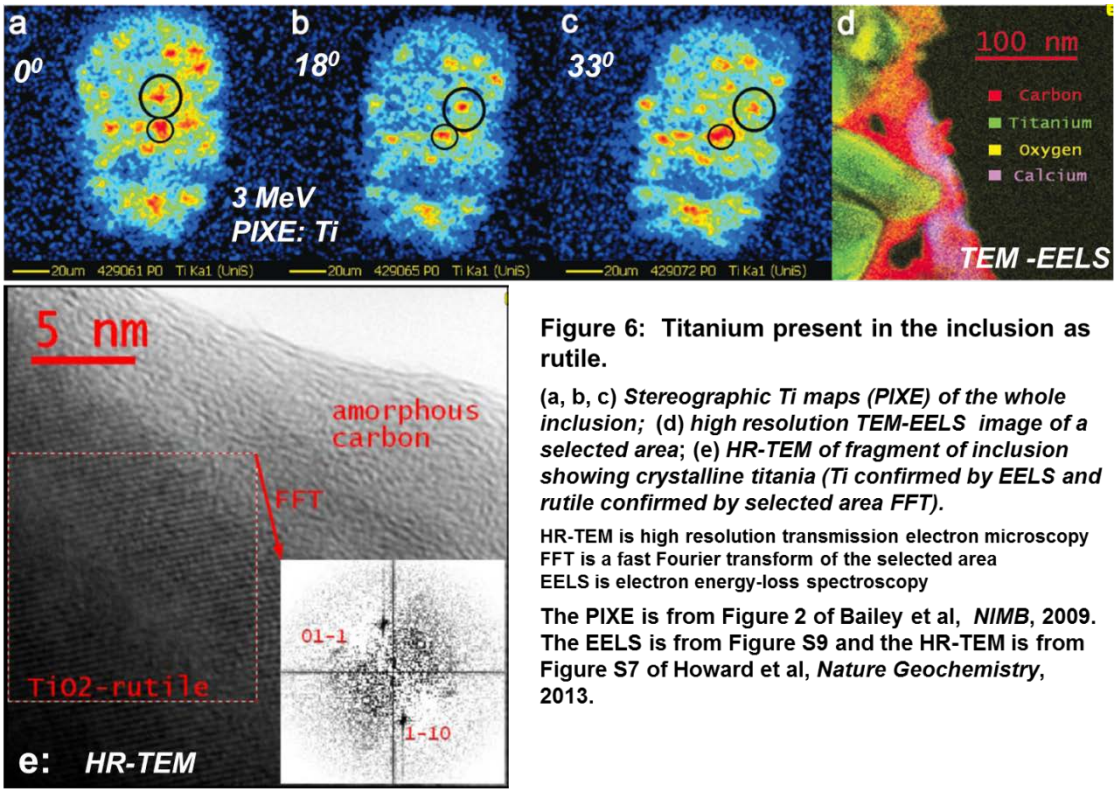

Figure 6: Titanium present in the inclusion as rutile.

(a, b, c) ***Stereographic Ti maps (PIXE) of the whole inclusion;*** **(d)** ***high resolution TEM-EELS image of a selected area*****; (e)** ***HR-TEM of fragment of inclusion showing crystalline titania (Ti confirmed by EELS and rutile confirmed by selected area FFT).***

HR-TEM is high resolution transmission electron microscopy
FFT is a fast Fourier transform of the selected area
EELS is electron energy-loss spectroscopy

The PIXE is from Figure 2 of Bailey et al, *NIMB*, 2009. The EELS is from Figure S9 and the HR-TEM is from Figure S7 of Howard et al, *Nature Geochemistry*, 2013.

Figure 6 shows a set of images of titanium in the whole inclusion (PIXE) through small (EELS) to tiny (HR-TEM) parts of it. The HR-TEM (phase contrast) image of the nanocrystalline rutile confirms the original XRD observation of quartz and rutile from the whole Darwin glass sample. The TEM samples were obtained by grinding the inclusion, dispersing the powder in water and filtering onto a holey TEM grid. Clearly the regions of interest are found serendipitously. This highlights the value of the IBA prior to using the very powerful TEM techniques: with IBA the representativeness of the TEM can be demonstrated. We can search in the TEM for interesting regions that we already know exist.

Quartz fragments were not found in the TEM (accidentally). But as for the rutile so also for the quartz: the rutile was proved by the TEM analysis to be co-genetic with the carbon, and thus we have an explanation for the presence of crystallites in this high temperature quenched material that ought to have been amorphous. Carbon (from the vaporised rainforest) was entrained by the condensing rock vapour into inclusions which are spherical to minimise surface energy in the usual way. The carbon is a good thermal insulator so that the cooling rate in the inclusion is much slower than the cooling rate for the bulk of the glass. Hence the existence of crystals.

This Case Study can be pressed further. The IBA dataset consists of *two* data "cubes": one for each detector (in this case PIXE and EBS). For each pixel of each map there is an energy spectrum (a histogram). Clearly the raw dataset is enormous: how to handle it?

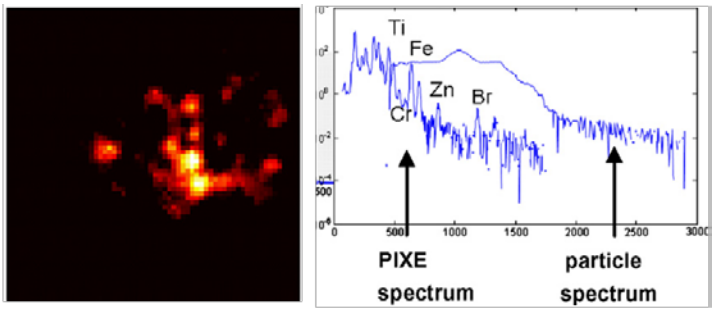

Figure 7: ***Principal component (PC) analysis of IBA data-cube***

The data-cubes of Figure 5 are decomposed into 7 PCs, where each PC consists of two spectra (PIXE & EBS) from a "selected area". The "area" for one of the PCs is shown (*left*), with the two spectra on a log scale (*right*).

From Figure 2 of Jeynes et al, *NIMB* 2009

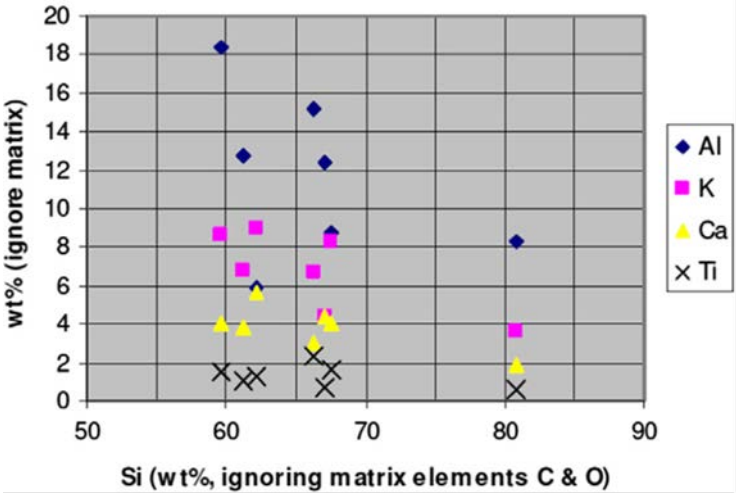

Figure 8: ***Refractory elements relative to Si (see PCA of Fig.6)***

The PIXE/EBS spectral pairs derived from the principal component analysis of the data-cube imaged in Fig.5 (see Fig.7) are fitted to obtain characteristic depth profiles for those components (see Fig.4), deriving elemental ratios with Si. Some of these data, for all seven PCs are shown here.

From Figure 3 of Jeynes et al, *NIMB* 2009

Figure 7 shows one component of a *principal component* analysis (Jeynes et al, *Nucl. Instruments & Methods B*, 2009 [4]): the pairs of spectra for the nine PCs can be fitted as for Figure 4. Selected results of such an analysis are shown in ***Figure 8*** for seven components. In principle, the depth profile at each pixel can be reconstructed from a linear combination of the principal components, and therefore the 3-D structure of the sample is completely solved.

Saying that the 3-D structure of the sample can be completely solved is equivalent to saying that the tomography problem is solved, but without making any projections! X-ray tomography is a solved problem (and we have shown an example here), and scanning transmission ion microscopy tomography (STIM-T [5]) is an equivalent (solved) problem. PIXE-T [6] is a more difficult problem but also (almost) solved.

The difficulty with PIXE-T is that because of the relatively low PIXE cross-sections the beam damage is not negligible, and because PIXE does not have direct depth information, PIXE-T requires large numbers of sections, dramatically increasing the dose – and damage! – incurred by the sample. Few samples are able to survive PIXE-T (for an example see Andrea et al, *Nucl. Instruments & Methods B*, 2010 [7]).

But IBA (PIXE+EBS) *does* have great depth sensitivity, and consequently only a few sections are necessary for tomography. This Example also effectively demonstrates the feasibility of what we might loosely call "IBA-T". In principle, using the depth information available explicitly in IBA-T (from the particle signals) *must* be quicker than unfolding the depth information available only implicitly (and at much lower resolution) in the PIXE signals.

Cited Literature

[1] Kieren Torres Howard, Melanie J. Bailey, Deborah Berhanu, Phil A. Bland, Gordon Cressey, Lauren E. Howard, Chris Jeynes, Richard Matthewman, Zita Martins, Mark A. Sephton, Vlad Stolojan, Sasha Verchovsky, Biomass preservation in implact melt ejecta, *Nature Geoscience*, **6** (2013) 1018-1022; DOI: 10.1038/ngeo1996.

[2] M.J. Bailey, K.T. Howard, K.J. Kirkby, Characterisation of inhomogeneous inclusions in Darwin glass using ion beam analysis, *Nuclear Instruments & Methods B*, **267** (2009) 2219-2224; DOI: 10.1016/j.nimb.2009.03.013.

[3] J.P. Stoquert, T. Szörényi, Determination of the number and size of homogeneities in thin films by ion beam analysis, *Physical Review B*, **66** (2002) 144108; DOI: 10.1103/PhysRevB.66.144108.

[4] C. Jeynes, M.J. Bailey, N.J. Bright, M.E. Christopher, G.W. Grime, B.N. Jones, V.V. Palitsin, R.P. Webb, "Total IBA" – where are we?, *Nuclear Instruments & Methods B*, **271** (2012) 107-118; DOI: 10.1016/j.nimb.2011.09.020.

[5] T. Satoh, M. Oikawa, T. Kamiya, Three-dimensional measurement of elemental distribution in minute samples by combination of in-air micro-PIXE and STIM, *Nuclear Instruments & Methods B*, **267** (2009) 2125-2127; DOI: 10.1016/j.nimb.2009.03.067.

[6] Chris G. Ryan, PIXE and the nuclear microprobe: tools for quantitative imaging of complex natural materials, *Nuclear Instruments & Methods B*, **269** (2011) 2151-2162; DOI: 10.1016/j.nimb.2011.02.046.

[7] T. Andrea, M. Rothermel, R. Werner, T. Butz, T. Reinert, Limited angle STIM and PIXE tomography of single cells, *Nuclear Instruments & Methods B*, **268** (2010) 1884-1888; DOI: 10.1016/j.nimb.2010.02.049.